JACS
JOURNAL OF THE AMERICAN CHEMICAL SOCIETY

Article

pubs.acs.org/JACS

Preparation of Core–Shell Coordination Molecular Assemblies via the Enrichment of Structure-Directing "Codes" of Bridging Ligands and Metathesis of Metal Units

Jinhee Park,[‡,∥,⊥] Ying-Pin Chen,[‡,§,⊥] Zachary Perry,[‡] Jian-Rong Li,*[,†,‡] and Hong-Cai Zhou*[,†,‡,§]

[†]Department of Chemistry and Chemical Engineering, College of Environmental and Energy Engineering, Beijing University of Technology, Beijing, 100124, P. R. China

[‡]Department of Chemistry, Texas A&M University, P.O. Box 30012, College Station, Texas 77842, United States

[§]Department of Materials Science and Engineering, Texas A&M University, College Station, Texas 77843, United States

[∥]Nano Hybrid Technology Research Center, Creative and Fundamental Research Division, Korea Electrotechnology Research Institute, Changwon 641-120, Republic of Korea

Supporting Information

ABSTRACT: A series of molybdenum- and copper-based MOPs were synthesized through coordination-driven process of a bridging ligand (3,3′-PDBAD, $\mathbf{L^1}$) and dimetal paddlewheel clusters. Three conformers of the ligand exist with an ideal bridging angle between the two carboxylate groups of 0° ($H_2\alpha$-$\mathbf{L^1}$), 120° ($H_2\beta$-$\mathbf{L^1}$), and of 90° ($H_2\gamma$-$\mathbf{L^1}$), respectively. At ambient or lower temperature, $H_2\mathbf{L^1}$ and $Mo_2(OAc)_4$ or $Cu_2(OAc)_4$ were crystallized into a molecular square with γ-$\mathbf{L^1}$ and Mo_2/Cu_2 units. With proper temperature elevation, not only the molecular square with γ-$\mathbf{L^1}$ but also a lantern-shaped cage with α-$\mathbf{L^1}$ formed simultaneously. Similar to how Watson–Crick pairs stabilize the helical structure of duplex DNA, the core–shell molecular assembly possesses favorable H-bonding interaction sites. This is dictated by the ligand conformation in the shell, coding for the formation and providing stabilization of the central lantern shaped core, which was not observed without this complementary interaction. On the basis of the crystallographic implications, a heterobimetallic cage was obtained through a postsynthetic metal ion metathesis, showing different reactivity of coordination bonds in the core and shell. As an innovative synthetic strategy, the site-selective metathesis broadens the structural diversity and properties of coordination assemblies.

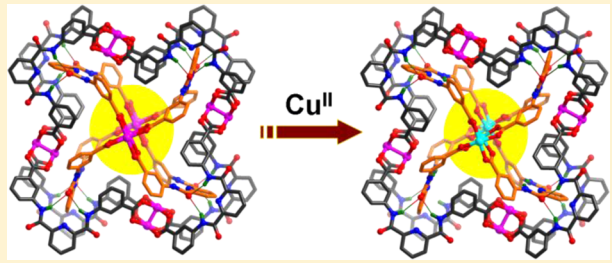

INTRODUCTION

Over the past two decades, coordination driven molecular self-assemblies have been studied extensively due to their beautiful structures, unique physical/chemical properties, and potential applications. Among such self-assembled structures, a variety of metal–organic polygons/polyhedra (MOPs) have been designed and synthesized, using inspirations drawn from not only geometric entities such as Archimedean and Platonic solids but also biological systems with high symmetry.[1−8] Both interior and exterior functionalizations[9−11] of MOPs have been carried out, allowing the isolation of the confined space to be explored toward molecular recognition,[10,12] sensing,[13] catalysis,[14−18] regioselective[19,20] and self-sorting reactions,[21] molecular flasks,[22,23] storage of reactive species,[24] and other potential applications.[24,25] Structures of the resulting MOPs are often controlled by the coordination geometry of the metal or metal units, and the bridging angles of the organic ligands.[1,5,25−29] Recently, a few new synthetic methods, such as bridging-ligand-substitution strategy and the use of mixed ligand systems, have been developed in our laboratory to expand the structural diversity of MOPs.[30,31] However, compared to natural systems, the structural complexity of MOPs is still limited; new strategies need to be developed to enrich MOP chemistry.

Nature utilizes a variety of weak interactions such as H-bonding, $\pi-\pi$ stacking, and hydrophobic interactions to build various biological systems with relatively simple building units containing structure-directing "codes". For example, DNA double strands are constructed based on Watson–Crick pairs which rely on complementary H-bonding interactions resulting from specific base pairs. In coordination driven molecular self-assemblies, the building blocks (organic linkers and metal-containing nodes) can be designed to possess structure-directing "codes" such as built-in multiple H-bonding interaction sites, intrinsic coordination modes, and variable coordination angles, leading to the formation of MOPs with desired structural features and functionalities.[1] As the "codes" directing the structure become more complicated, the complexity of the coordination assembly will increase.

Herein, we report a series of MOPs, including novel core–shell coordination molecular assemblies, derived from dimetal

Received: August 26, 2014
Published: November 10, 2014

   dx.doi.org/10.1021/ja508822r | J. Am. Chem. Soc. 2014, 136, 16895−16901

paddlewheel units (Cu_2 and Mo_2 units) and multiple conformers of organic linkers, 3,3′-((pyridine-2,6-dicarbonyl)-bis(azanediyl))dibenzoate (3,3′-PDBAD, $\mathbf{L}^1$, Figure 3a) and its positional isomer 4,4′-((pyridine-2,6-dicarbonyl)bis-(azanediyl))dibenzoate (4,4′- PDBAD, $\mathbf{L}^2$, Figure 3b). The protonated ligand $H_2\mathbf{L}^1$ was synthesized from the condensation reaction of 2,6-pyridinedicarbonyl dichloride and 3-amino-benzoic acid via the formation of amide bonds, which are well-known for H-bonding interactions with H-bond donors and acceptors. Three conformers of $H_2\mathbf{L}^1$ exist, namely *anti*−*anti* (designated $H_2\alpha$-$\mathbf{L}^1$ for simplicity) with an ideal bridging angle between the two carboxylate groups of 0°, *syn*−*syn* ($H_2\beta$-$\mathbf{L}^1$) with a bridging angle of 120°, and *anti*−*syn* ($H_2\gamma$-$\mathbf{L}^1$) of 90° bridging angle (Figure 1). In principle, $H_2\beta$-$\mathbf{L}^1$ and $H_2\gamma$-$\mathbf{L}^1$ have

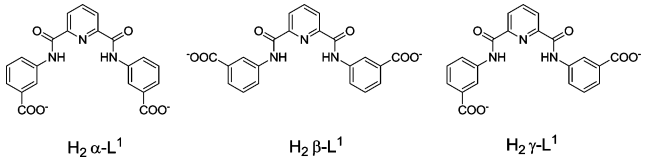

Figure 1. Three different conformers of 3,3′-H_2PDBAD, $\mathbf{L}^1$.

less steric hindrance than $H_2\alpha$-$\mathbf{L}^1$. It is thus anticipated that at low temperature, $H_2\beta$-$\mathbf{L}^1$ and $H_2\gamma$-$\mathbf{L}^1$ may dominate because they are energetically favorable; in contrast, all conformers can coexist at high temperature. Unfortunately, we did not observe β-$\mathbf{L}^1$ throughout the experiments.

In this context (schemed in Figure 2), at low temperature the reaction between $H_2\mathbf{L}^1$ and $Mo_2(OAc)_4$ or $Cu_2(OAc)_4$ gave rise to a molecular square with γ-$\mathbf{L}^1$ and Mo_2 or Cu_2 units.[32] When the temperature was elevated, both a lantern-shaped cage with α-$\mathbf{L}^1$ and a molecular square with γ-$\mathbf{L}^1$ formed simultaneously. The cage was encapsulated inside the square through multipoint H-bonding interactions. The enrichment of structure-directing "codes" of the bridging ligand has thus resulted in the formation of a unique core−shell coordination molecular assembly, where a metal−organic polyhedron is encapsulated inside a metal−organic polygon. This strategy may have general implications in the synthesis of more complicated coordination assemblies, including molecular and extended structures. The formation of a double shell structure was reported by Fujita and co-workers,[33] where linkers consisting of dual bispyridines were adopted, leading to the formation of a sphere-in-sphere complex by "orthogonal" self-assembly. Clever and co-workers demonstrated an interpenetrated dimeric cage, showing allosteric binding ability of halide anions.[34] As for the present system, a molecular square and cage are nested to form a core−shell structure via multipoint H-bonding interactions, reminiscent of H-bonding interactions in the Watson−Crick pairs of a DNA double helix.

RESULTS AND DISCUSSION

A molybdenum-based molecular square, $[Mo_2(\gamma\text{-}\mathbf{L}^1)_2(DEF)_2]_4\cdot S$ (**1**, *S* represents uncoordinated solvent molecules) was isolated as yellow plate crystals from the reaction of $H_2\mathbf{L}^1$ and $Mo_2(AcO)_4$ in *N*,*N*-diethylformamide (DEF) at room temperature for 2 days under a N_2 atmosphere. Similarly, a reaction between $H_2\mathbf{L}^1$ and $Cu_2(AcO)_4(H_2O)_2$ in *N*,*N*-dimethylacetamide (DMA) at 4 °C for 2 days afforded green octahedral crystals of $[Cu_2(\gamma\text{-}\mathbf{L}^1)_2(DMA)_2]_4\cdot S$ (**2**), the Cu^{2+} analogue of **1**. The structures of **1** and **2** were determined by single-crystal X-ray diffraction analysis. Compounds **1** and **2** are almost

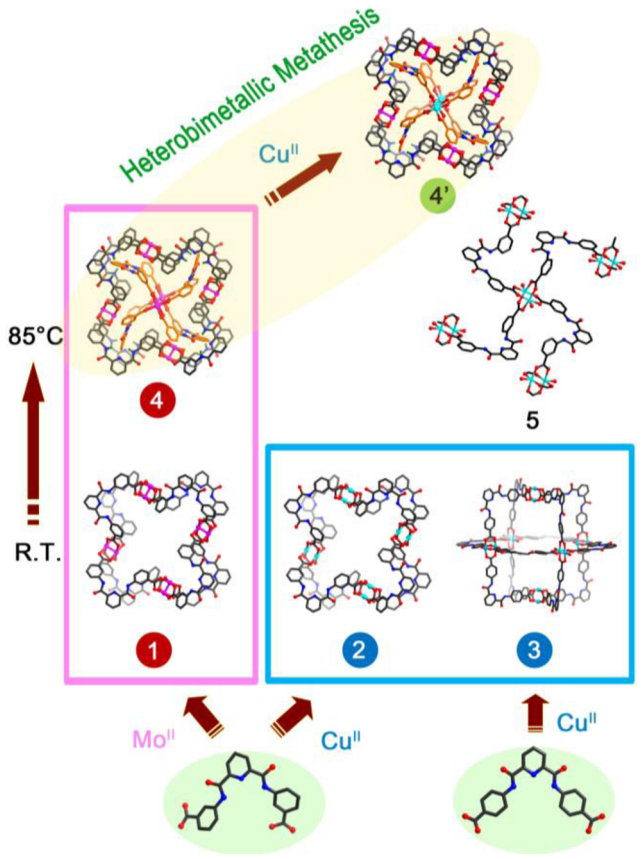

Figure 2. Overview scheme of all self-assembled structures in this work.

isostructural except the following minor differences. The former is sitting on a 4/*m* site and has crystallographically imposed C_{4h} symmetry, while the compound **2** has C_{2h} symmetry. The packing between MOPs is most affected by the coordinated solvent molecules which change distance between individual MOPs in the structures. The top views and side views of the two close-packed structures can be found in Supporting Information Figures S7 and S8. Both are derived from four untwisted M_2 paddlewheel units coordinated by four pairs of γ-$\mathbf{L}^1$ ligands, whose conformation is kinetically trapped at low temperature (see Figure 3a,c). It is also worth mentioning that the interior surface of the molecular square is functionalized with 16 amide groups and four Mo_2 (or Cu_2) units, which may enable their utility in cooperative catalysis.[35]

When the isomeric bridging ligand, $\mathbf{L}^2$ (4,4′-PDBAD, Figure 3b), instead of $\mathbf{L}^1$ (3,3′-PDBAD, Figure 3a) was assembled with Cu_2 units, an octahedral cage (Figure 3d), $[Cu_2(\mathbf{L}^2)_2(DMA)_2]_6\cdot S$ (**3**) was afforded. MOP **3** has a structure similar to the previously reported molecular octahedron, $[Cu_2(CDC)_2]_6$, where a carbazole dicarboxylate ligand, 9*H*-carbazole-3,6-dicarboxylate (CDC) with a 90° bridging angle was used.[36] In **3**, the ligand $\mathbf{L}^2$ also adopts a conformation with an approximately 90° bridging angle as shown in Figure 3b. Twelve $\mathbf{L}^2$ ligands act as edges bridging six Cu_2 vertices giving rise to the octahedral cage. The internal cavity size (referring to the diameter of the largest sphere that can be accommodated within the cage) and the edge length of a triangular window in the octahedral cage are 20.18 and 14.10 Å, respectively. A comparison between **2** (the Cu_2 analogue of **1**) and **3** indicates that even with the same bridging angle and the same metal

dx.doi.org/10.1021/ja508822r | J. Am. Chem. Soc. 2014, 136, 16895−16901

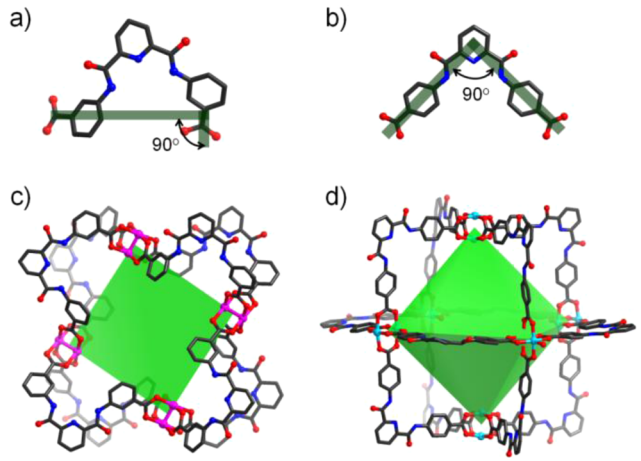

Figure 3. Structures of molecular assemblies **1** (c) and **3** (d) as well as their 90° bridging-angle ligands, $\mathbf{L^1}$ (a) and $\mathbf{L^2}$ (b), respectively (H atoms of ligands and coordinated solvent molecules were omitted for clarity). Color scheme: Mo, pink; Cu, cyan; O, red; N, blue; C, black. The green polygon and polyhedron represent geometries of **1** and **2** when considering metal clusters as vertices and ligands as edges.

node, the structures of the resulting molecular architectures (herein the molecular square and octahedral cage) can be totally different if the ligands contain intrinsically different structure-directing codes.

Although **1**−**3** all contain carboxamide groups in their organic linkers, MOP **3** is not soluble in common organic solvents. MOPs **1** and **2**, on the other hand, are soluble in DMA and DEF, respectively, allowing the study of their solution absorption spectra (Supporting Information Figure S29). The absorption spectrum of **1** in DMA exhibits a characteristic peak at 450 nm, corresponding to the $\delta \rightarrow \delta^*$ transition of the Mo−Mo quadruple bond.[37] Because the Mo_2 unit is sensitive to oxidation, the spectroscopic feature gradually diminishes in air (Supporting Information Figure S30). The absorption spectrum of **2** in DEF displays a feature at 713 nm as shown in Supporting Information Figure S29. In addition, preliminary CO_2 sorption studies at 195 K were performed with activated solid-state samples of **1** and **2** to confirm their porosity (Supporting Information Figure S31). The BET and Langmuir surface areas of **1** are 92.9 and 282.34 m^2/g, and those of **2** are 139 and 471 m^2/g, respectively.

In an attempt to induce conformational changes of $\mathbf{L^1}$ (thus observe either α- or β-conformation), the reaction mixture of $H_2\mathbf{L^1}$ and $Mo_2(AcO)_4$ in DMA was heated to 85 °C under a N_2 atmosphere. After 2 days, light yellow crystals of $[Mo_2(\gamma\text{-}\mathbf{L^1})_2(DMA)_2]_4[Mo_2(\alpha\text{-}\mathbf{L^1})_2(DMA)_2]_2{\cdot}S$ (**4**) were harvested and its structure was solved by single-crystal X-ray diffraction analysis. As expected, an additional conformer, α-$\mathbf{L^1}$, was found in a coordination molecular assembly. Unexpectedly this assembly was nested inside of the γ-$\mathbf{L^1}$ bridged square (Figure 4). As shown in Figure 4c, four α-$\mathbf{L^1}$ ligands bridges two Mo_2 units, leading to a lantern-shaped molecular cage (the "core"). The inner cavity size of the cage is 6.52 Å (distance between the two inner Mo ions of the Mo_2 units) × 16.43 Å (distance between the two nitrogen atoms in the two pyridyl rings of the two opposite α-$\mathbf{L^1}$ ligands).[38] The γ-$\mathbf{L^1}$ ligands form a molecular square (the "shell") identical to **1**. The lantern shape molecular cage is encapsulated inside the square, yielding a core−shell assembly (**4**). Assembly **4** exhibits C_{4h} symmetry, with a 4-fold axis passing through the Mo−Mo quadruple bond.

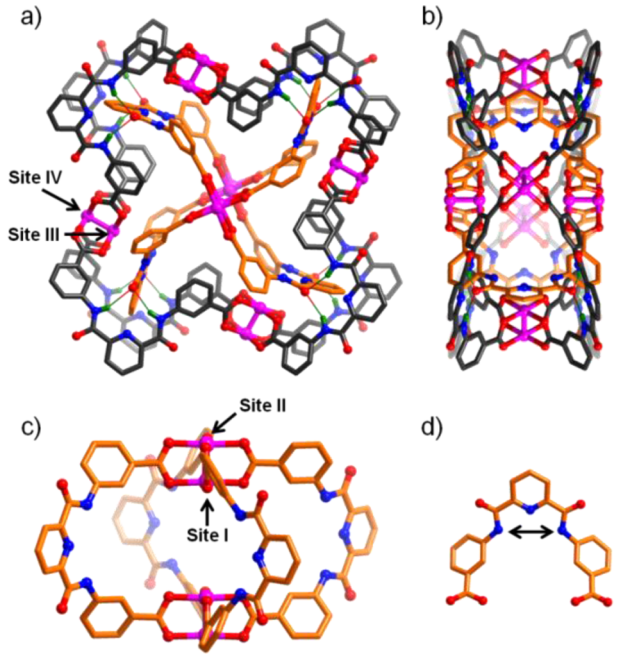

Figure 4. (a) and (b) Structure of the core−shell molecular assembly **4** viewed from the *c* direction and *a*/*b* directions, respectively (H-bond interactions are shown in thin green/red bonds); (c) structure of the core molecular cage in **4**; and (d) α-$\mathbf{L^1}$ in the core of **4** (non-H-bonding H atoms of ligands and coordinated solvent molecules were omitted for clarity). Panels a and c also show sites I, II, III, and IV of Mo_2 units. Color scheme: Mo, pink; O, red; N, blue; H, dark green; C, black (in shell) or orange (in core).

Sixteen H-bonds (shown in green/red thin line segments in Figure 4a) between the core and shell have formed, demonstrating the power of the structure directing "codes", which facilitate the formation of the core−shell structure and stabilize the overall structure (Figure 4a,b). Attempted syntheses of a stand-alone core structure or a Cu_2-based core−shell analogue were unsuccessful. In fact, at an elevated temperature the mixture of Cu^{2+} ions and $H_2\mathbf{L^1}$ formed a two-dimensional (2-D) coordination polymer, **5**, in which the $\mathbf{L^1}$ ligands adopt the γ conformation (Supporting Information Figure S9).

Interestingly, we were able to utilize the core−shell structure **4** to prepare a heterobimetallic molecular assembly via metathesis of the metal units. Metathesis has been widely used to prepare relatively stable molecular assemblies by replacing more labile metal ions with other metal ions by forming kinetically inert coordination bonds.[39,40] However, the metathesis of MOPs in the form of single crystal to single crystal transformation has been, to the best of our knowledge, unreported likely due to their structural instability and low porosity which could restrict ion flow in such single crystals. In **4**, two types of distinct Mo_2 units, one in the core and the other in the shell are coordinated with two different conformers of $\mathbf{L^1}$. Metal ion metathesis in a single crystal to single crystal transformation can elucidate the reactivity difference of these coordination bonds through the crystal structure analysis. Crystals of freshly synthesized **4** were immersed in a 0.1 M $Cu(NO_3)_2$ solution in *N*,*N*-dimethylformamide (DMF) under an Ar atmosphere for 6 and 48 h. [With longer immersion time (2 weeks), the crystals of **4** became amorphous, indicating compound decomposition or transformation. This prevented the structural determination at longer exchange times.] On the

dx.doi.org/10.1021/ja508822r | J. Am. Chem. Soc. 2014, 136, 16895−16901

basis of energy-dispersive X-ray spectroscopic studies (EDS), Cu/Mo molar ratios for Cu^{2+} exchanged **4** (denoted as **4′**) remained the same (1:1.1) after 6 or 48 h of exchange reaction (Supporting Information Table S2). Cu and Mo mapping revealed homogeneous metathesis throughout the crystals (Supporting Information Figure S15). This partial metathesis suggests that some of the Mo_2 units in **4** undergo exchange with the Cu_2 units readily but the rest are too inert to undergo metal metathesis under given conditions. Note that the same metathesis conditions (even after 5 days only a very small amount of uptake ∼5% was seen, which, without convincing X-ray analysis, we are unable to accredit to this exchange mechanism) are unsuccessful for other 3d transition metals, such as Mn^{2+}, Co^{2+}, Ni^{2+}, Zn^{2+} ions (Supporting Information Table S3). We have attributed this process to the relatively slow exchange rates[41] as well as preferred coordination geometry and the stability of the resulting dimetal paddlewheels. Therefore, we will focus on the Cu^{2+} exchanged **4** in this work.

To investigate where and how the metathesis occurred, the structure of **4′** was characterized by single-crystal X-ray diffraction analysis (Figure 5a, right), which revealed that the heterobimetallic assembly, $[Mo_2(\gamma\text{-}\mathbf{L}^1)_2]_4[Cu_2(\alpha\text{-}\mathbf{L}^1)_2]_2{\cdot}S$ (**4′**) was the final product (Figure 5a). In the structure of **4′**, the interatomic distances of the M_2 units in the core and shell structures are 2.560 Å (2.100 Å before metathesis) and 2.217 Å (2.099 Å before metathesis), respectively. On the basis of CCDC database, 2.560 Å is the typical distance from Cu to Cu in a Cu−Cu paddle wheel (2.6 Å); in contrast, 2.217 Å is similar to Mo−Mo quadruple bond length (2.1 Å). The torsional angles around the metal ions of the core and shell structure are 15.50° (0.09° before metathesis) and 2.63° (0.01° before metathesis), respectively (Figure 5b,c). These observations indicate that the Mo_2 units in the core cage were almost replaced by the Cu_2 units, while those in the shell were partially substituted.[42]

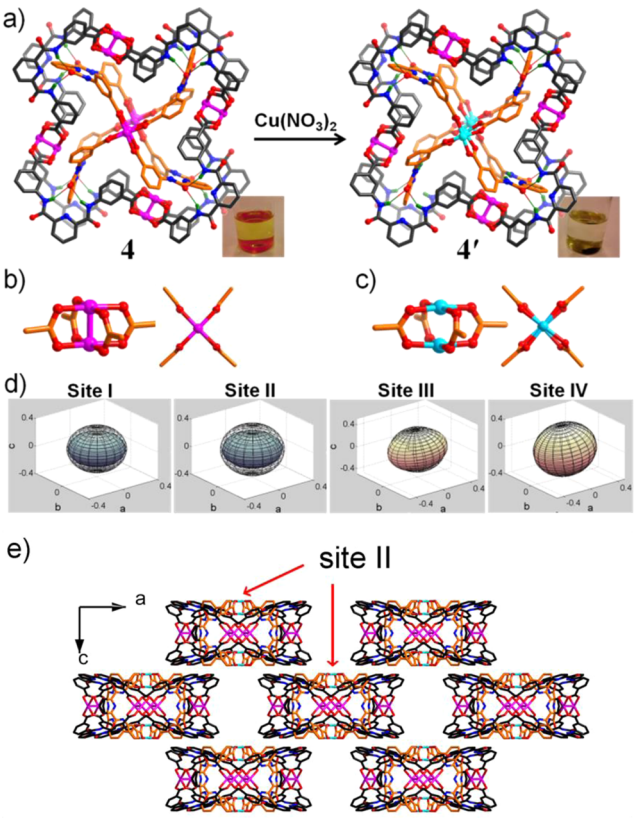

Figure 5. (a) Metal ion metathesis in core−shell assembly **4** to give **4′**. Photographs show the color change of the crystals from red orange to dark green during the metathesis; (b and c) views of the paddlewheel metal-carboxylate centers in the core cages of **4** and **4′**, respectively. Color scheme: Mo, pink; Cu, cyan; O, red; N, blue; H, black green; C, black (in shell) or orange (in core). (d) Thermal ellipsoids before (colored) after metathesis (transparent) at sites I, II, III, and IV. (e) The close packed structure of **4′** viewed along −*b* axis.

The core-selective metathesis observed in this work could be attributed to the several reasons. First, a close inspection of the packing of the core−shell structure from both the crystallographic *a* and *b* directions reveals that the site II of the Mo_2 units in the core is directly accessible from a 1-D channel (Figure 5e). Even with axial ligands on the two Mo atoms, there is still enough space for solvated Cu^{2+} ions to easily reach the Mo_2 units, which is why the exchange reaction is fast. In fact, once the Cu salt was added, an immediate color change of the crystal was observed. The M_2 units in the shell (sites III and IV), on the other hand, are not directly accessible due to the coordinated ligands. We postulate that during the metathesis reaction, the quadruply bonded Mo_2 units must be solvated and then Cu^{2+} ions replace them. The excess Cu^{2+} ions could then participate in the shell metathesis. The shell metathesis, however, was not complete. Once the 1:1.1 molar ratio of Cu/Mo has been reached, either elongating the reaction time (2 weeks) or increasing the concentration of Cu^{2+} solution did not lead to further metathesis. This phenomenon can be described by a process of thermodynamic equilibrium. It has been reported that metal centers connected by flexible ligand environments can participate in competing equilibria due to environmental conditions and cation identity.[43,44] For the core, the α-$\mathbf{L}^1$ ligand produces stress on the Mo_2 units, which energetically favors relatively flexible Cu_2 units to release their tension. We believe the quadruply bonded Mo−Mo species, which is positionally locked due to orbital symmetry, prevents the release of this tension. As there is no bond in the Cu_2 unit, the torsional strain can be relieved by a twist in the core conformation. In contrast, the shell possesses less stress than the core does thus a partial substitution between the Mo_2 units and Cu^{2+} ions is enough to release their tension.

Anisotropic atomic displacement parameters (ADP, $U_{ij,}$) of the metals in **4** and **4′** were analyzed in order to confirm the complete metathesis in the core and partial one in the shell. ADP, namely, thermal ellipsoids, could be regarded as spreading of electron diffusion around their equilibrium positions on account of positional disorder, inverse-proportionally reflecting confinement of atoms[45−47] (see details in Supporting Information section 2.4). It can be quantified and compared by the ellipsoid volumes proportional to multiplicity of eigenvalues of the ADP matrices (eq (2.5.9) in Supporting Information). In Figure 5d, the volume of thermal ellipsoids before metathesis at site III and site IV is obviously larger than that at site I and site II. Since the thermal ellipsoids reflect local flexibility of a structure, which is potentially related to the reactivity,[46,47] Figure 5d implies that the reactivity of the four sites is different (Supporting Information Figure S11). As a result, the Mo_2 units at sites I and II have constrained thermal motion of the electrons, like a compressed spring, thus being more reactive. Graphically, the shape of the thermal ellipsoids at sites I and II transformed from flat ellipsoids to spherical ellipsoids after metathesis, indicating a release of the torsional

dx.doi.org/10.1021/ja508822r | J. Am. Chem. Soc. 2014, 136, 16895−16901

strain along *c*-axis. In addition, the H-bonds stabilized the core structure during the metal substitution process, resulting in the selective substitution of the core without the collapse of the cage. It should be pointed out that the direct synthesis for such a heterobimetallic molecular assembly from Cu^{2+} and Mo^{2+} mixtures yielded amorphous powders. Consequently, the core−shell assembly can be used as a template for other hereobimetallic molecular assemblies. The site-specific metal substitution provides a good synthetic strategy to broaden the structures of coordination driven molecular assemblies, which are difficult to access through the direct assembly process. Furthermore, the preparation of the heterobimetallic molecular assemblies is a meaningful step in realization of enzyme-mimetic supramolecules. In biological systems, various heterometallic complexes are involved in cooperative enzymatic reactions.[48,49]

■ CONCLUSIONS

We have reported a series of the MOPs, including the core−shell molecular assemblies derived by the building blocks (organic linkers and meal-containing nodes) possessing the right structure-directing "codes" to facilitate the formation of unfavorable conformations. The core−shell MOP was successfully employed as a template to prepare a heterobimetallic assembly, in which the metal metathesis occurred favorably in the core. The site-selective metal metathesis provides a novel synthetic strategy to broaden the structures and properties of coordination assemblies, including molecular and extended structures. Synthetic strategies to take full advantage of the built-in structure-directing codes to attain more complicated molecular assemblies are currently being developed in our laboratory.

■ EXPERIMENTAL SECTION

Instruments. ^{1}H nuclear magnetic resonance (NMR) data was used to confirm the ligand syntheses, recorded on a Mercury 300 spectrometer at the Center for Chemical Characterization and Analysis (CCCA). FT-IR analysis was conducted by use of an IRAffinity-1 instrument. The TGA data was obtained in a TGA-50 (SHIMADZU) thermogravimetric analyzer with a heating rate of 5 °C/min under 25 mL/min N_2 flow. Single crystal reflections were collected on a Bruker single-crystal APEXII CCD Diffractometer with Mo Kα (λ = 0.71073 Å) at 110 K. The powder X-ray diffraction patterns (PXRD) were recorded by a Bruker D8-Focus Bragg−Brentano X-ray Powder diffractometer equipped with a Cu sealed tube (λ = 1.54178 Å) at a scan rate of 0.5 s deg^{-1}. Gas adsorption measurements were performed by Micromeritics' ASAP 2020 with extra-pure quality gases. Molar ratio of copper and molybdenum of 4′ was determined by ICP-MS (Agilent 7700x) analysis and SEM-EDS (FEI Quanta 600) equipped with X-ray mapping and digital imaging. Vacuum dried powdery **4**′ was dissolved in 200 μL of 30% trace-metal grade HNO_3 (Fisher Scientific), and diluted up to 8 mL with deionized H_2O for ICP analysis.

Chemicals. Copper acetate monohydrate, copper nitrate, 2,6-pyridinedicarboxylic acid, 3-aminobenzoic acid, 4-aminobenzoic acid, molybdenumhexacarbonyl, thionyl chloride, *N*,*N*-diethylformamide, and 2,6-lutidine were purchased from Alfa Aesar Chemicals. Acetonitrile and glacial acetic acid were supplied by BDH. *N*,*N*-Dimethylacetamide was obtained from Acros organic. *N*,*N*-Dimethylformamide was obtained from Macron fine chemicals. All starting materials were used as received without further purification.

Synthesis of 3,3′-H_2PDBAD, L^1. 2,6-Pyridinedicarboxylic acid (2.0 g, 12.0 mmol) and thionyl chloride (40.0 mL, 0.55 mol) were mixed in a dried 250 mL round-bottomed flask. *N*,*N*-Dimethylformamide (1.0 mL, 12.9 mmol) was carefully added dropwise, and the mixture was stirred and heated at 75 °C for 6 h under N_2 flow. The excess thionyl chloride was removed under vacuum and quenched with ethanol and then water. Due to the reactivity of 2,6-pyridinedicarbonyl chloride, the residual 2,6-pyridinedicarbonyl chloride was used without further purification. 2,6-Pyridinedicarbonyl chloride (0.61 g, 3.0 mmol) was dissolved in 20 mL of anhydrous acetonitrile and added dropwise to a solution of 3-aminobenzoic acid (0.96 g, 7.0 mmol) in acetonitrile (20 mL). The resulting mixture was stirred at room temperature for 24 h and then refluxed for 2 h. The precipitated white solid was isolated by filtration and washed with 100 mL of acetonitrile followed by 500 mL of water and then overnight drying under vacuum. Yield for the two steps: 0.98 g, 81%. ^{1}H NMR (300 MHz, DMSO-d_6) δ 11.19 (s, 2 H), 8.56 (s, 2 H), 8.45 (d, 2 H, J = 7.2 Hz), 8.34 (t, 1 H, J = 7.6 Hz), 8.20 (d, 2H, J = 8.1 Hz). IR (ν max): 3379, 3329, 2816, 1678, 1604, 1589, 1519, 1454, 1408, 1315, 1288, 1242, 1184, 1118, 999, 933, 891, 856, 767, 740, 686 cm^{-1}. Elemental Analysis (% calc/found): C, 62.22/62.09; H, 3.73/3.76; N, 10.37/10.41. (Supporting Information Figures S1−S3)

Synthesis of 4,4′-H_2PDBAD, L^2. L^2 was isolated from the same procedure except using 4-aminobenzoic acid instead of 3-aminobenzoic acid. Yield of 0.96 g, 79% for two steps. ^{1}H NMR (300 MHz, DMSO-d_6) δ 11.28 (s, 2 H), 8.46 (d, 2 H, J = 7.5 Hz), 8.34 (t, 1 H, J = 7.5 Hz), 8.13 (d, 2 H, J = 7.8 Hz), 8.05 (d, 2H, J = 7.8 Hz). IR (ν max): 3286, 3228, 2808, 1697, 1658, 1589, 1554, 1531, 1438, 1292, 1230, 1138, 1080, 999, 948, 898, 813, 756, 736, 659 cm^{-1}. Elemental Analysis (% calc/found): C, 62.22/61.97; H, 3.73/3.60; N, 10.37/10.20. (Supporting Information Figure S4 ∼ S6)

$Mo_2(OAc)_4$ Synthesis. Under nitrogen, 2.99 g of $Mo(CO)_6$ (11.3 mmol) was added to a stirring mixture of 100 mL glacial acetic acid and 20 mL acetic anhydride. A vacuum was applied and the flask was backfilled with nitrogen; this was repeated three times. The solution was allowed to reflux for 32 h. At this point, stirring was stopped and the flask was allowed to cool overnight, yielding crystals which appeared to be green in color. After washing three times with ethanol, the now bright yellow crystals were dried under reduced pressure. Yield: 1.0176 g (2.2 mmol), 39%.

Synthesis of $[Mo_2(\gamma\text{-}L^1)_2(DEF)_2]_4$·*S* 1. A mixture of H_2L^1 (20 mg), $Mo(OAc)_2$ (20 mg), and *N*,*N*-diethylformamide (DEF) (1.5 mL) was placed in a 2 mL vial. The vial was purged with N_2 and allowed to sit in room temperature for 2 days. Yellow block crystals of **1** were obtained. IR (ν max): 3313, 3078, 1681, 1589, 1531, 1392, 1303, 1222, 1141, 1076, 979, 910, 840, 810, 756, 678 cm^{-1}. Elemental Analysis of activated **1** (% calc/found): C, 50.52/46.92; H, 2.62/3.66; N, 8.42/9.01.

Synthesis of $[Cu_2(\gamma\text{-}L^1)_2(DMA)_2]_4$·*S* 2. H_2L^1 (8 mg), $Cu(OAc)_2$ (8 mg), and *N*,*N*-dimethylacetamide (DMA) (1.5 mL) were added 2 mL vial. The reaction took place at 4 °C for 2 days. Green block crystals were collected. IR (ν max): 3294, 3078, 1678, 1531, 1431, 1392, 1307, 1222, 1145, 1080, 999, 910, 837, 759, 678 cm^{-1}. Elemental Analysis of activated **2** (% calc/found): C, 54.02/51.72; H, 2.81/4.58; N, 9.00/11.02.

Synthesis of $[Cu_2(L^2)_2(DMA)_2]_6$·*S* 3. 2,6-Lutidine (0.1 mL) was added to the mixture of H_2L^2 (40 mg), $Cu(NO_3)_2$ (25 mg), and DMA (15 mL) in 20 mL vial. The reaction took place at room temperature in 1 day. Blue plate crystals were collected. IR (ν max): 3260, 3101, 1662, 1600, 1527, 1384, 1315, 1176, 1110, 1080, 1014, 860, 779, 744, 682 cm^{-1}. Elemental Analysis of activated **3** (% calc/found): C, 54.02/50.65; H, 2.81/3.86; N, 9.00/8.97.

Synthesis of $[Mo_2(\gamma\text{-}L^1)_2(DMA)_2]_4[Mo_2(\alpha\text{-}L^1)_2(DMA)_2]_2$·*S* 4. A mixture of H_2L^1 (20 mg) and $Mo(OAc)_2$ (20 mg) in 1.5 mL of DMA was prepared in a 2 mL vial, purged with N_2, and heated to 85 °C for 2 days. Light red block crystals were isolated. IR (ν max): 3290, 3082, 1658, 1589, 1531, 1388, 1300, 1222, 1138, 1076, 956, 914, 840, 813, 756, 675 cm^{-1}. Elemental Analysis of **4** (% calc/found): C, 50.52/48.14; H, 2.62/3.82; N, 8.42/8.73.

Metal Ion Metathesis for Cu−Core Mo−Shell $[Mo_2(\gamma\text{-}L^1)_2]_4[Cu_2(\alpha\text{-}L^1)_2]_2$·*S* 4′. Due to the oxygen sensitivity of Mo^{2+} complexes, the entire sample preparation steps were conducted in an Ar atmosphere glovebox. The as-synthesized single crystals of **4** were briefly washed with fresh DMF. Approximately 20 mg of the crystals **4** was soaked in 2 mL of 100 mM $Cu(NO_3)_2$ in DMF for 6 h,

dx.doi.org/10.1021/ja508822r | J. Am. Chem. Soc. 2014, 136, 16895−16901

Table 1. Crystal Data and Results of Structure Refinement

	1	2	3	4	4′	5
	Mo shell	Cu shell	octahedral cage	Mo core−shell	Mo core/Cu shell	Cu 2D sheet
CCDC	953691	953692	953693	953694	953695	953696
Formula	$Mo_8C_{168}H_{104}N_{24}O_{56}$	$Cu_8C_{168}H_{104}N_{24}O_{56}$	$Cu_{12}C_{252}H_{156}N_{36}O_{84}$	$Mo_{12}C_{252}H_{156}N_{36}O_{80}$	$Cu_{5.6}Mo_{6.4}C_{252}H_{156}N_{36}O_{78}$	$Cu_2C_{58}H_{62}N_{10}O_{16}$
Formula weight	4122.27	3863.07	5794.61	6119.41	5905.97	1282.26
Color/Shape	Orange Octahedron	Green Octahedron	Blue Square plates	Yellow Rod	Green Rod	Green Chunk
Crystal system	Tetragonal	Orthorhombic	Triclinic	Tetragonal	Tetragonal	Monoclinic
Space group	*I*4/*m*	*Cmce*	$P\bar{1}$	*I*4/*m*	*I*4/*m*	$P2_1/c$
a (Å)	34.623(2)	23.524(5)	26.273(5)	31.220(10)	31.22(3)	8.9180(12)
b (Å)	34.623(2)	31.791(7)	26.687(5)	31.220(10)	31.22(3)	15.890(2)
c (Å)	16.4266(10)	48.797(10)	29.106(6)	24.656(8)	25.05(3)	20.734(3)
α (deg)	90.00	90.00	90.067(3)	90.00	90.00	90.00
β (deg)	90.00	90.00	108.930(2)	90.00	90.00	97.404(2)
γ (deg)	90.00	90.00	105.381(2)	90.00	90.00	90.00
V (Å^3)	19691(2)	36493(13)	18527(6)	24032(14)	24416(44)	2913.6(7)
Z	2	4	1	2	2	2
$d_{calcd.}$ (g/cm^3)	0.695	0.703	0.519	0.846	0.803	1.462
μ (mm^{-1})	0.287	0.501	0.370	0.352	0.446	0.809
F(000)	4128	7840	2940	6128	5950	1332
θ_{max} [deg]	26.00	26.00	24.98	24.00	24.82	26.00
Completeness	99.9%	99.5%	97.8%	99.7%	98.2%	100.0%
Collected reflections	103537	94146	132545	86231	25881	21574
Unique reflections	10019	18320	63673	9669	10619	5724
Parameters	261	245	679	237	176	411
Restraints	15	39	116	21	23	9
R_{int}	0.0741	0.0802	0.1041	0.1934	0.1836	0.0706
*R*1 [$I > 2\sigma(I)$]	0.0626	0.1591	0.0815	0.1353	0.1434	0.0441
*wR*2 [$I > 2\sigma(I)$]	0.1625	0.3077	0.1519	0.2555	0.2659	0.0764
*R*1 (all data)	0.0881	0.2137	0.2168	0.2542	0.3304	0.0872
*wR*2 (all data)	0.1693	0.3287	0.1634	0.2847	0.3150	0.0832
GOF on F^2	1.002	1.009	0.880	0.994	1.004	1.005
$\Delta\rho_{max}/\Delta\rho_{min}$ [e·Å^{-3}]	2.753/−0.938	2.006/−1.030	0.751/−0.776	1.319/−0.780	1.136/−0.705	0.810/−0.808

1 day, 2 days, and 20 days. During the soaking process, the solution was refreshed with fresh $Cu(NO_3)_2$ solution every day. Single crystal X-ray diffraction analysis was performed on the crystals directly taken out from the solution without further washing process. For EDS analysis, the solution was exchanged with fresh DMF for 2 days to remove any remaining residues. These same conditions were applied to the nitrate salts of Mn, Co, Ni, and Zn, which showed no metathesis after 2 days by EDS analysis.

Single Crystal X-ray Crystallography. All MOP crystals were mounted onto a loop from mother liquid for single crystal X-ray data collection without further treatment. Diffractions were measured on a Bruker Smart Apex diffractometer equipped with a Mo−Kα sealed-tube X-ray source (λ = 0.71073 Å) and liquid nitrogen stream (110 K). The data frames were recorded using the program APEX2 and processed using the program *SAINT* (v7.68A) routine within APEX2 (v2012.2.0). Absorption and beam corrections based on the multiscan technique were applied to the integrated data using *SADABS* (v2008/1). All the structures were solved by direct method using *SHELXS* and refined by full-matrix least-squares on F^2 using *SHELXL* software.

Carbon atoms with enormous thermal ellipsoids were refined with the help of EADP restrains on each ligand to clear the warnings about nonpositive definite matrices. All non-hydrogen atoms needed to be refined with anisotropic displacement parameters during the final cycles. Organic hydrogen atoms were located in calculated positions with isotropic displacement parameters set to 1.2 × U_{eq} of the attached atoms. The solvent molecules were highly disordered, and attempts to locate and refine the solvent peaks were not always successful. Contributions to scattering due to these solvent molecules were removed using the *SQUEEZE* routine of *PLATON*;[50] structures were then refined again using the data generated. . The refinement details and validation reply can be found in Supporting Information (section 2.1). The CIF files can be obtained free of charge from the Cambridge Crystallographic Data Centre via www.ccdc.cam.ac.uk/data_request/cif. CCDC numbers and the crystal information are listed in Table 1.

■ ASSOCIATED CONTENT

Supporting Information

Crystallography data and figures of the MOPs and the coordination polymer. Calculations of atomic displacement parameters of the MOPs. SEM-EDS, FT-IR, PXRD, TGA, UV−vis, and CO_2 adsorption data of MOPs. This material is available free of charge via the Internet at http://pubs.acs.org.

■ AUTHOR INFORMATION

Corresponding Authors

zhou@tamu.edu

jrli@bjut.edu.cn

Author Contributions

⊥These authors contributed equally.

Notes

The authors declare no competing financial interest.

■ ACKNOWLEDGMENTS

J. Park was supported through Energy Frontier Research Center funded by U.S. Department of Energy (DE-SC0001015). Y.-P. Chen was partially paid on U.S. Department of Energy (DE-FC36-07GO17033) and partially on National

Science Foundation (NSF CBET-0930079). Z. Perry thanks the support of the U.S. Department of Energy ARPA-e (DE-AR0000249) and the Office of Naval Research (N00014-13-1-0753) as well as Texas A&M University. J.-R. Li -thanks the support from the Natural Science Foundation of China (No. 21271015, 21322601), the Program for New Century Excellent Talents in University (No. NCET-13-0647), and the Beijing Municipal Natural Science Foundation (No. 2132013). H.-C. Zhou gratefully acknowledges support from U.S. Department of Energy (DE-SC0001015, DE-AR000073, and DE-FC36-07GO17033). The synthesis and characterization of the molecular squares reported here were funded by U.S. Department of Energy (DE- SC0001015, DE-AR000073, and DE-FC36-07GO17033) and Welch Foundation grant (A-1725). The FE-SEM acquisition was supported by the NSF grant DBI-0116835, the VP for research office, and the TX Eng. Exp. Station. The authors thank Dr. Paul Lindahl for the performance and valuable discussions on ICP-MS analysis.

REFERENCES

(1) Chakrabarty, R.; Mukherjee, P. S.; Stang, P. J. *Chem. Rev.* **2011**, *111*, 6810−6918.
(2) Cook, T. R.; Zheng, Y.-R.; Stang, P. J. *Chem. Rev.* **2012**, *113*, 734−777.
(3) Sun, Q.-F.; Sato, S.; Fujita, M. *Nat. Chem.* **2012**, *4*, 330−333.
(4) Han, Y.; Li, J.-R.; Xie, Y.; Guo, G. *Chem. Soc. Rev.* **2014**, *43*, 5952−5981.
(5) Tranchemontagne, D. J.; Ni, Z.; O'Keeffe, M.; Yaghi, O. M. *Angew. Chem., Int. Ed.* **2008**, *47*, 5136−5147.
(6) Prakash, M. J.; Lah, M. S. *Chem. Commun.* **2009**, 3326−3341.
(7) Perry, J. J., IV; Perman, J. A.; Zaworotko, M. J. *Chem. Soc. Rev.* **2009**, *38*, 1400−1417.
(8) Fujita, M.; Yazaki, J.; Ogura, K. *J. Am. Chem. Soc.* **1990**, *112*, 5645−5647.
(9) Hamilton, T. D.; Papaefstathiou, G. S.; Friščić, T.; Bučar, D.-K. i.; MacGillivray, L. R. *J. Am. Chem. Soc.* **2008**, *130*, 14366−14367.
(10) Fang, Y.; Murase, T.; Sato, S.; Fujita, M. *J. Am. Chem. Soc.* **2012**, *135*, 613−615.
(11) Schmidtendorf, M.; Pape, T.; Hahn, F. E. *Angew. Chem., Int. Ed.* **2012**, *51*, 2195−2198.
(12) Nakamura, T.; Ube, H.; Shiro, M.; Shionoya, M. *Angew. Chem., Int. Ed.* **2013**, *52*, 720−723.
(13) Clegg, J. K.; Cremers, J.; Hogben, A. J.; Breiner, B.; Smulders, M. M. J.; Thoburn, J. D.; Nitschke, J. R. *Chem. Sci.* **2013**, *4*, 68−76.
(14) Pluth, M. D.; Bergman, R. G.; Raymond, K. N. *Science* **2007**, *316*, 85−88.
(15) Pluth, M. D.; Bergman, R. G.; Raymond, K. N. *Angew. Chem., Int. Ed.* **2007**, *46*, 8587−8589.
(16) Hastings, C. J.; Pluth, M. D.; Bergman, R. G.; Raymond, K. N. *J. Am. Chem. Soc.* **2010**, *132*, 6938−6940.
(17) Brown, C. J.; Miller, G. M.; Johnson, M. W.; Bergman, R. G.; Raymond, K. N. *J. Am. Chem. Soc.* **2011**, *133*, 11964−11966.
(18) Lu, W.; Yuan, D.; Yakovenko, A.; Zhou, H.-C. *Chem. Commun.* **2011**, *47*, 4968−4970.
(19) Kumazawa, K.; Biradha, K.; Kusukawa, T.; Okano, T.; Fujita, M. *Angew. Chem.* **2003**, *115*, 4039−4043.
(20) Yoshizawa, M.; Tamura, M.; Fujita, M. *Science* **2006**, *312*, 251−254.
(21) Smulders, M. M. J.; Jiménez, A.; Nitschke, J. R. *Angew. Chem., Int. Ed.* **2012**, *51*, 6681−6685.
(22) Yoshizawa, M.; Klosterman, J. K.; Fujita, M. *Angew. Chem., Int. Ed.* **2009**, *48*, 3418−3438.
(23) Osuga, T.; Murase, T.; Fujita, M. *Angew. Chem., Int. Ed.* **2012**, *51*, 12199−12201.
(24) Mal, P.; Breiner, B.; Rissanen, K.; Nitschke, J. R. *Science* **2009**, *324*, 1697−1699.
(25) Ni, Z.; Yassar, A.; Antoun, T.; Yaghi, O. M. *J. Am. Chem. Soc.* **2005**, *127*, 12752−12753.
(26) Northrop, B. H.; Zheng, Y.-R.; Chi, K.-W.; Stang, P. J. *Acc. Chem. Res.* **2009**, *42*, 1554−1563.
(27) Cotton, F. A.; Lin, C.; Murillo, C. A. *Acc. Chem. Res.* **2001**, *34*, 759−771.
(28) Eddaoudi, M.; Kim, J.; Wachter, J. B.; Chae, H. K.; O'Keeffe, M.; Yaghi, O. M. *J. Am. Chem. Soc.* **2001**, *123*, 4368−4369.
(29) Smulders, M. M. J.; Riddell, I. A.; Browne, C.; Nitschke, J. R. *Chem. Soc. Rev.* **2013**, *42*, 1728−1754.
(30) Li, J.-R.; Zhou, H.-C. *Nat. Chem.* **2010**, *2*, 893−898.
(31) Li, J.-R.; Zhou, H.-C. *Angew. Chem., Int. Ed.* **2009**, *48*, 8465−8468.
(32) Cotton, F. A.; Daniels, L. M.; Lin, C.; Murillo, C. A. *J. Am. Chem. Soc.* **1999**, *121*, 4538−4539.
(33) Sun, Q.-F.; Murase, T.; Sato, S.; Fujita, M. *Angew. Chem., Int. Ed.* **2011**, *50*, 10318−10321.
(34) Freye, S.; Hey, J.; Torras-Galán, A.; Stalke, D.; Herbst-Irmer, R.; John, M.; Clever, G. H. *Angew. Chem., Int. Ed.* **2012**, *51*, 2191−2194.
(35) Park, J.; Li, J.-R.; Chen, Y.-P.; Yu, J.; Yakovenko, A. A.; Wang, Z. U.; Sun, L.-B.; Balbuena, P. B.; Zhou, H.-C. *Chem. Commun.* **2012**, *48*, 9995−9997.
(36) Li, J.-R.; Timmons, D. J.; Zhou, H.-C. *J. Am. Chem. Soc.* **2009**, *131*, 6368−6369.
(37) Radius, U.; Breher, F. *Angew. Chem., Int. Ed.* **2006**, *45*, 3006−3010.
(38) Li, J.-R.; Yakovenko, A. A.; Lu, W.; Timmons, D. J.; Zhuang, W.; Yuan, D.; Zhou, H.-C. *J. Am. Chem. Soc.* **2010**, *132*, 17599−17610.
(39) Kim, Y.; Das, S.; Bhattacharya, S.; Hong, S.; Kim, M. G.; Yoon, M.; Natarajan, S.; Kim, K. *Chem.—Eur. J.* **2012**, *18*, 16642−16648.
(40) Das, S.; Kim, H.; Kim, K. *J. Am. Chem. Soc.* **2009**, *131*, 3814−3815.
(41) Helm, L.; Merbach, A. E. *Chem. Rev.* **2005**, *105*, 1923−1960.
(42) Chisholm, M. H. *Proc. Natl. Acad. Sci. U.S.A.* **2007**, *104*, 2563−2570.
(43) Cui, X.; Khlobystov, A. N.; Chen, X.; Marsh, D. H.; Blake, A. J.; Lewis, W.; Champness, N. R.; Roberts, C. J.; Schröder, M. *Chem.—Eur. J.* **2009**, *15*, 8861−8873.
(44) Aime, S.; Botta, M.; Fasano, M.; Marques, M. P. M.; Geraldes, C. F. G. C.; Pubanz, D.; Merbach, A. E. *Inorg. Chem.* **1997**, *36*, 2059−2068.
(45) Friedman, R.; Caflisch, A. *Proteins: Struct., Funct., Bioinf.* **2008**, *73*, 814−827.
(46) Yuan, Z.; Zhao, J.; Wang, Z.-X. *Protein Eng.* **2003**, *16*, 109−114.
(47) Gana, R.; Rao, S.; Huang, H.; Wu, C.; Vasudevan, S. *BMC Struct. Biol.* **2013**, *13*, 6−20.
(48) Sasai, H.; Arai, T.; Satow, Y.; Houk, K. N.; Shibasaki, M. *J. Am. Chem. Soc.* **1995**, *117*, 6194−6198.
(49) Anaya de Parrodi, C.; Walsh, P. J. *Angew. Chem., Int. Ed.* **2009**, *48*, 4679−4682.
(50) Sheldrick, G. M. *SHELXTL*, Version 6.14, Structure Determination Software Suite, Bruker AXS: Madison, WI, 2003.